PRECISION ELECTROWEAK RESULTS AT LEP-I AND LEP-II

Manel Martinez
Institut de Fisica d'Altes Energies, Edifici Cn, U. A. B.
E-08193 Bellaterra (Barcelona), Spain

ABSTRACT

The most relevant LEP electroweak measurements obtained during the LEP-I and LEP-II operation phases are briefly reviewed, and their internal consistency, as well as their agreement with the Minimal Standard Model (MSM) predictions, are discussed.

1 Introduction

Since its start-up in 1989, LEP has proven to be the most powerful machine to probe the theory of the electroweak interactions, the MSM. A full bunch of high precision measurements performed by the four LEP experiments allow now the extraction of many important parameters to an unprecedented level of accuracy.

With the start of the LEP-II program in fall 1995, the LEP-I program arrived to its end although, as of now, part of the LEP-I data has not yet reached final publication. The reason for that is that several measurements have been reanalyzed in the light of a better theoretical and experimental understanding of the systematic effects. Nevertheless, altogether the LEP-I measurements have been already the subject of many good and extensive reviews (see, for instance Ref. 1) and therefore, in spite of their great importance, in this note we are going to omit the details about their experimental determination and discuss just the results, their meaning, and their interpretation. On the contrary, we want to describe in some more detail the LEP-II results which, apart from being more recent, have now just started reaching maturity.

In this note, the most relevant LEP Electroweak measurements performed so far are briefly presented, paying special attention to their systematic limitations, and their impact in the Standard Model (SM). The results presented here come, for most observables, from all data taken between 1989 and 1997 by the four LEP experiments: about 15 million hadronic Z decays and about 1.7 million charged-lepton Z decays coming from the Z resonance scan, together with about 4000 W pair events coming from the WW production at and above threshold. Most of the results discussed are still preliminary although they have been already presented in public.[2]

The Z observables are classified into three groups: Z lineshape and lepton forward-backward asymmetry measurements, tau polarization measurements, and finally, electroweak results with quarks, where the present results, analyzed together with the ones obtained at SLAC, have originated some discussion about possible systematic effects in the quark couplings to the Z, as we shall see later. The WW measurements are classified into three groups as well: WW cross section and branching ratios, the W mass, and the triple gauge couplings.

They are all discussed in turn in the following sections.

2 The LEP-I Measurements

2.1 Z Lineshape and Lepton F-B Asymmetry Measurements

The cross section for the production of a fermion pair $f\bar{f}$ can be written as

$$\sigma_{f\bar{f}}(s) = \int_{4m_f^2}^{s} ds' H(s,s') \hat{\sigma}_{f\bar{f}}(s') \,, \tag{1}$$

where $H(s,s')$ is the so-called radiator function which takes care of initial state radiation corrections, and the reduced cross section $\hat{\sigma}$ is written as

$$\hat{\sigma}_{f\bar{f}}(s) = \sigma^0_{f\bar{f}} \cdot \frac{s\Gamma_Z^2}{\left(s - M_Z^2\right)^2 + \left(s\Gamma_Z/M_Z\right)^2} + (\gamma - Z) + |\gamma|^2 \,, \tag{2}$$

where $\sigma^0_{f\bar{f}}$ is called the peak cross section, $\Gamma_Z = \Gamma_h + \Gamma_e + \Gamma_\mu + \Gamma_\tau + \Gamma_{inv}$ stands for the total Z width, and M_Z is the Z mass. This parameterization assumes the validity of QED for the photon exchange part and also takes from the MSM the interference between the photon- and Z-mediated amplitudes. * This interference is very small around the Z pole. In the case of Bhabha scattering, $f = e$, one can either subtract from the data the t-channel contributions, also taken from the theory, or add them to the previous expression. The cross section at the peak can be written in turn in terms of the Z mass and width, and the Z partial widths to the initial state Γ_e and the final state Γ_f:

$$\sigma^0_{f\bar{f}} = \frac{12\pi}{M_Z^2} \cdot \frac{\Gamma_e \Gamma_f}{\Gamma_Z^2} \,, \tag{3}$$

where the partial widths can be written in terms of effective vector and axial couplings of the fermions to the Z:

$$\Gamma_l = \frac{G_F M_Z^3}{6\pi\sqrt{2}} \left({g_{V_l}}^2 + {g_{A_l}}^2\right) \left(1 + \frac{3\alpha}{4\pi}\right) \,. \tag{4}$$

Assuming lepton universality, only four parameters are needed to describe the s-dependence of the hadronic and leptonic cross sections: M_Z, Γ_Z, σ^0_h, and the ratio of hadronic to leptonic partial widths ($R_l = \Gamma_h/\Gamma_l = \sigma^0_h/\sigma^0_l$), where the lepton is taken to be massless. If lepton universality is not assumed, R_l is substituted by three analogous quantities, R_e, R_μ, and R_τ. This choice of parameters, given the fact that they are directly related to geometrical characteristics of the lineshape, has two advantages: on the one hand, their correlations are small, and on the other hand they simplify the task of disentangling common uncertainties:

*For some experiments, this is only the case for hadronic final states.

- M_Z and Γ_Z are the only measurements sensitive to the energy scale and they are strongly affected by common LEP energy uncertainties which, thanks to the use of the resonant depolarization technique for the determination of the LEP energy, have been reduced to 1.7 MeV and 1.3 MeV respectively.[3] The present LEP averages are $M_Z = 91.1867 \pm 0.0021$ GeV and $\Gamma_Z = 2.4939 \pm 0.0024$ GeV.
- σ_h^0 is the only lineshape observable in which the overall normalization, and hence the luminosity measurement uncertainties, enter. Presently this measurement is already dominated by the common systematical error due to the theoretical uncertainty in the low-angle Bhabha cross section, which presently is estimated to be of 0.11% (Ref. 4). Since R_l is a ratio of cross sections, the luminosity measurement cancels and there is, so far, no relevant source of common systematics affecting it sizably. The present LEP averages are $\sigma_h^0 = 41.491 \pm 0.058$ nb and $R_l = 20.765 \pm 0.026$.

The forward-backward asymmetry is defined as

$$A_{FB} = \frac{\sigma_F - \sigma_B}{\sigma_F + \sigma_B}, \tag{5}$$

where F and B indicate the forward or backward hemisphere. Normally it is obtained by fitting the measured angular distribution to the formula

$$\frac{d\sigma^l}{d\cos\theta}(s) = \frac{3}{8}\sigma^l(s) \cdot \left(1 + \cos^2\theta + \frac{8}{3}A_{FB}^l(s)\cos\theta\right) . \tag{6}$$

In the case of the e^+e^- final state, the t-channel contribution is either subtracted from the observed asymmetry or added to the previous expression.

Once the different $A_{FB}^l(s_i)$ are obtained, they are fitted together with the lineshape data to get the lineshape parameters mentioned above and the peak asymmetry, $A_{FB}^{0,l}$:

$$\begin{aligned} A_{FB}^{0,l} &= \frac{3}{4}A_e A_l \\ A_f &= \frac{2g_{V_f}/g_{A_f}}{1 + \left(g_{V_f}/g_{A_f}\right)^2}. \end{aligned} \tag{7}$$

from which the effective weak mixing angle is measured. The main error in this measurement is still statistical. Experimental systematics can only come from simultaneous charge and forward-backward asymmetries in the detector, which are bound to be very small. The present knowledge of the beam energy contributes a non-negligible 0.0005 to $\Delta A_{FB}^{0,l}$. The LEP average for the peak asymmetry is $A_{FB}^{0,l} = 0.01683 \pm 0.00096$.

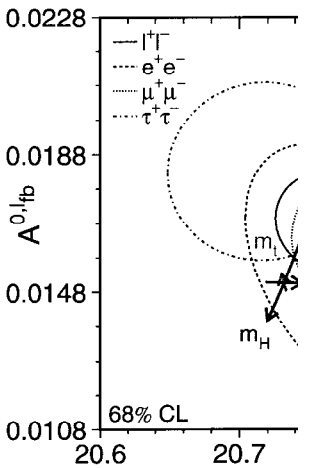

Fig. 1. Contours of 68% probability in the R_l- to correspond to a massless lepton. Unless note the arrows showing the Standard Model $m_t = 173.8 \pm 5.0$ GeV, $M_H = 300\ ^{+700}_{-210}$ GeV, in the direction of increasing values.

Figure 1 summarizes the tests for lepton uni' forward-backward lepton asymmetry analyses

The use of the sketched procedure does in rameterization of the lineshape and asymmetr contribution to the hadronic cross section, bec dividually measured for each flavor. This tern general approach, which is to parameterize th the Z exchange amplitude, has been implem so-called S-matrix ansatz.[5] Fitting the LEP-I

center-of-mass energies between 130 and 172 GeV in that approach, the Z mass as defined above turns out to be $M_Z = 91.1882 \pm 0.0031$ and the parameter which measures the hadronic γZ interference turns out to be $j^{tot}_{had} = 0.14 \pm 0.14$ in good agreement with the MSM expectation $j^{tot}_{had} = 0.22$ (Ref. 2).

2.2 Tau Polarization

The measurement of the final state longitudinal polarization asymmetry for tau leptons:

$$< P_\tau > = \frac{\sigma_R - \sigma_L}{\sigma_R + \sigma_L} = -A_\tau, \tag{8}$$

where $\sigma_{R(L)}$ is the integrated cross section for right (left) handed taus, provides a means to measure the tau couplings to the Z directly. Since the taus decay inside the detectors, their helicity information can be obtained by using their parity-violating weak decays as a spin analyzer. The main decays used are: electron, muon, pion, rho, and a_1. Maximal sensitivity is obtained for the semileptonic modes (pion and rho) since then just one neutrino escapes detection. In this case, the decay angle of the hadron in the tau rest frame (or equivalently its scaled energy) is measured and the integrated tau polarization is extracted from

$$\frac{1}{N}\frac{dN}{dx} = 1 + \alpha < P_\tau > \cos\theta^* , \tag{9}$$

where α is a sensitivity coefficient linked to the spin of the hadron. For pions ($s = 0$), $\alpha = 1$, and for ρ and a_1 ($s = 1$), $\alpha < 1$, but α can be improved by studying the hadron helicity through the analysis of its decay products. The systematics are in this case comparable to the statistical errors and their eventual reduction would require a lot of effort in the further understanding of the calorimeters.

By measuring the tau polarization as a function of the tau production angle, θ one can write

$$P_\tau(\cos\theta) = -\frac{A_\tau + A_e \cdot \frac{2\cos\theta}{1+\cos^2\theta}}{1 + A_e A_\tau \cdot \frac{2\cos\theta}{1+\cos^2\theta}} . \tag{10}$$

From this expression it is apparent that, while the integrated polarization measures A_τ, its forward-backward asymmetry measures the electron coupling, A_e.

The present LEP average results for these two measurements are $A_\tau = 0.1431 \pm 0.0045$ and $A_e = 0.1479 \pm 0.0051$.

This last measurement can be directly compared with the left-right initial state polarization asymmetry from SLD[6] since, in a rather model independent way, both determine the same quantity: $A^0_{LR} = A_e$. The SLD measurement $A_e = 0.1504 \pm 0.0023$ turns out to be in perfect agreement with the LEP average.

2.3 Electroweak Results with Quarks

Given the lack of techniques to tag the light quark flavors efficiently, most of the LEP experiments compute inclusively the forward-backward asymmetry in all hadronic events by estimating the average quark charge via a momentum-weighted mean of charges of the hadrons belonging to each quark's jet. This way, the inclusive forward-backward asymmetry for the actual Z decay mixture of quark flavors, or Quark Charge Asymmetry $< Q_{FB} >$ can be extracted leading to a LEP average of $\sin^2\theta^{lept}_{eff} = 0.2321 \pm 0.0010$. This uncertainty is dominated by the Monte Carlo modeling for light quarks.

The measurement of the Z decay width into b hadrons is especially important because, within the MSM, it receives a vertex correction involving the top quark, which is absent from any other final state. By taking the ratio $R_b = \Gamma_b/\Gamma_h$, most of the vacuum polarization corrections depending on the top quark and the Higgs mass cancel out, and one is left with the following approximate expression:

$$R_b \simeq R_d \cdot \left[1 - \frac{20}{13}\frac{\alpha}{\pi}\left(\frac{m_t^2}{M_Z^2} + \frac{13}{6}\log\frac{m_t^2}{M_Z^2}\right)\right] . \tag{11}$$

Therefore, R_b has a singular role since its accurate measurement should provide an indirect determination of m_t independent of M_H, which is something that none of the rest of precision measurements can do. Anyway, the effect of the top quark vertex corrections is only of order 2% for a top mass of 150 GeV. Therefore, only a precise measurement, to better than 1%, is useful to get information on the top mass.

The relatively large b mass ($\sim$ 4.7 GeV) and lifetime ($\sim 1.5 \times 10^{-12}$ s), makes possible the use of its decay kinematics to have the largest identification efficiency and purities among all the quarks. Several methods have been used to tag b events at LEP:

- Lepton tag: It uses high p and high p_t leptons from b decays. High purity can be achieved but one has to pay for the small semileptonic b branching ratio.
- Event shape tag: High mass, high momentum b mesons, or baryons give rise to particular event shapes which have been used to tag b events with high efficiency although rather modest purity. Recognition has been optimized using Neural Network techniques.
- Lifetime tag: The long lifetime of the b quark can be used, using silicon microvertex detectors, to tag b events by looking for tracks not coming from the Z production vertex. This is currently the best performing method with both high purity and efficiency.

The main systematic errors come from the evaluation of the efficiency and the background of the selection. The best option is to try to use data to estimate both. In practice, the techniques mentioned above can be used to tag only one hemisphere and look at the other one to measure the tag efficiency and the background. This is the basic idea of the "double tag" methods, in which these quantities are obtained from the measurement of the number of the tagged hemispheres N_t and double-tagged events N_{tt} through the following equations:

$$\begin{aligned} N_t &= 2N_{had}(R_b\varepsilon_b + R_c\varepsilon_c + (1 - R_b - R_c)\varepsilon_{uds}) \\ N_{tt} &= N_{had}(R_b\varepsilon_b^2 C_b + R_c\varepsilon_c^2 C_c \\ &\quad +(1 - R_b - R_c)\varepsilon_{uds}^2 C_{uds}) \,, \end{aligned} \tag{12}$$

where ε_i stand for the efficiencies [ε_b is of $\mathcal{O}(25\%)$ with lifetime tag, ε_c typically $\mathcal{O}(0.5\%)$ so that the typical b purity is of $\mathcal{O}(95\%)$ and ε_{uds} are negligible] and C_i are the tagging efficiency hemisphere correlations [typically $\mathcal{O}(1)$]. To solve these equations, R_b and ε_b are taken to be the unknowns while the rest of the quantities are computed using Monte Carlo simulation. Given the high purity of the lifetime tags,

$$\begin{aligned} R_b &\approx N_t^2/(4N_{tt}N_{had}) \\ \varepsilon_b &\approx 2N_{tt}/N_t \end{aligned} \tag{13}$$

and therefore, the uncertainty in the additional quantities determined with Monte Carlo, enters R_b in the following way:

$$\begin{aligned} \Delta R_b/R_b &\approx -1.5 \;\; \Delta\varepsilon_c/\varepsilon_b \\ \Delta R_b/R_b &\approx \Delta C_b \end{aligned} \tag{14}$$

so that, for instance, an absolute error of 1% on C_b translates directly into a 1% relative error on R_b. Given the fact that disentangling in the Monte Carlo the different correlation sources and their actual size is a rather difficult task, the estimation of their actual systematic uncertainty is being reanalyzed in some detail and, its final understanding might produce still sizable changes in the actual measurements. The present results from the four collaborations are shown in Fig. 2.

The c quarks can be tagged in two different ways:

- using b tag techniques (lepton tag, event shape), extending them to the lower p and p_t regions, and then fitting simultaneously the b and c information,
- through the reconstruction of charmed meson decays. The cleanest one is $D^{*+} \rightarrow$

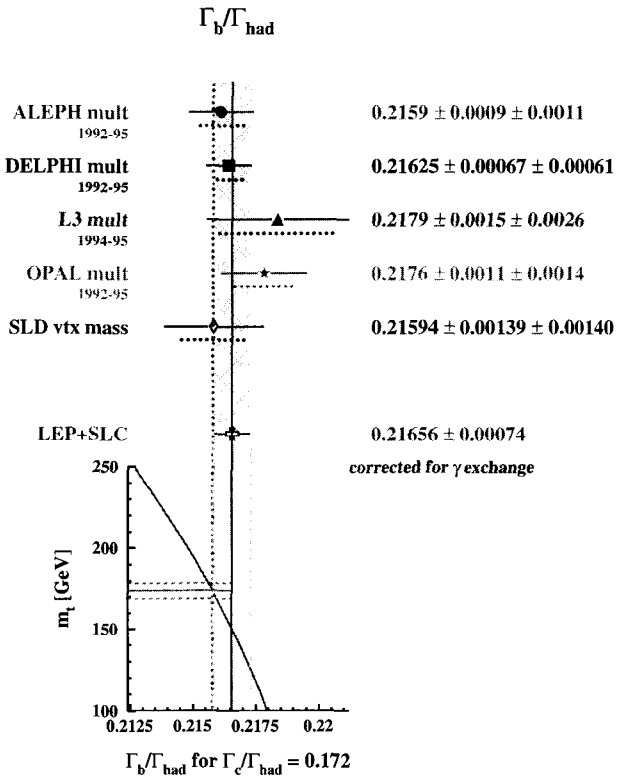

Fig. 2. The ratio of the Z partial width to b hadrons to the one to all hadrons measured by the four experiments, together with the mean and the MSM prediction as a function of the top quark mass. The error bars reflect the full uncertainty.

$D^0\pi^+$ and then $D^0 \to K^-\pi^+$ and its charge conjugate, because the low $D^* - D^0$ mass difference produces the signature of a soft π accompanying a D^0 with opposite charge to the K.

In either case, the efficiencies and purities are much lower than for b quarks and the dependence on external input for the production and decay branching ratios are very important. The results from the four collaborations are shown in Fig. 3, where one can see that the agreement between the different measurements is excellent. Usually the selection cuts are chosen to optimize the ratio between statistical and systematical uncertainties and, in this sense, these measurements are not systematically limited. At any rate, the weight of correlated systematical uncertainties is very important in the final errors and therefore, the proper averaging of the measurements from the different experiments and using different techniques is non-trivial. A detailed discussion, which also applies to the heavy flavor asymmetries to be presented later, can be found in Ref. 7. The improvement in the tag purities in the final analyses of the data have reduced the contamination of b events into the c sample and vice versa, leading to a correlation between the final averages of R_b and R_c of about –0.17.

The heavy quark forward-backward asymmetries provide presently the most precise determination of the effective weak mixing angle at LEP. What is measured is

$$A_{FB}^{0,q} = \frac{3}{4} A_e A_q \,, \tag{15}$$

where A_q is $\sim 0.66, 0.93$ for c- and b-type quarks, respectively, and depends only mildly on $\sin^2\theta_{eff}^{lept}$. Therefore, the asymmetry is quite large and mainly sensitive to the $\sin^2\theta_{eff}^{lept}$ dependence of A_e. The main difficulties measuring the forward-backward asymmetry for quark final states are the flavor identification and the charge assignment.

For b quarks, the charge assignment is done in two different ways: (i) either the charge of a high p, high p_t lepton from semileptonic decays, which identifies the b events, is also used to extract the charge of the parent quark, or (ii) the lifetime information in one hemisphere is used to tag the event while the weighted mean charge (jet charge) in the other hemisphere measures the quark charge. The two methods lead to samples which are almost completely statistically independent. The systematical errors differ as well: in the first method, the knowledge of the lepton purities and of the semi-leptonic branching ratios is crucial; in the second, the charm background in the b sample is the main worry, though, as in the case of the measurement of R_b, a lot of effort has been put by the LEP collaborations in redoing it as much as possible for the final analyses. The results obtained by the four LEP c methods explained can be seen in Fig. 4.

For c quarks, the charge is extracted either fom th global fits using the low p_t leptons from semiletonic

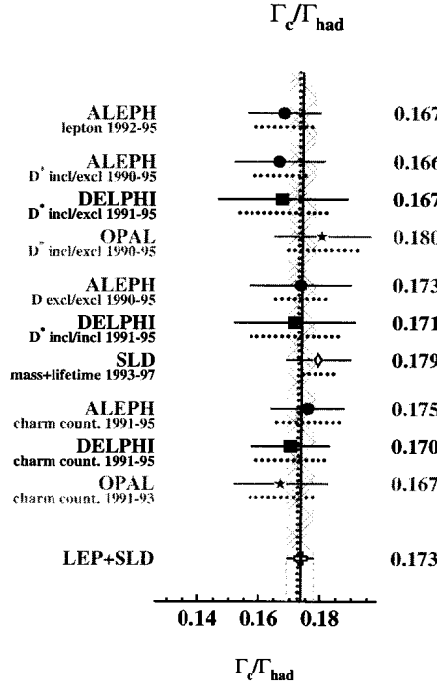

Fig. 3. The ratio of the Z partial width to c hadros to th by the four experiments, together with the mean ɛd the of the top quark mass. The error bars reflect the fil unc

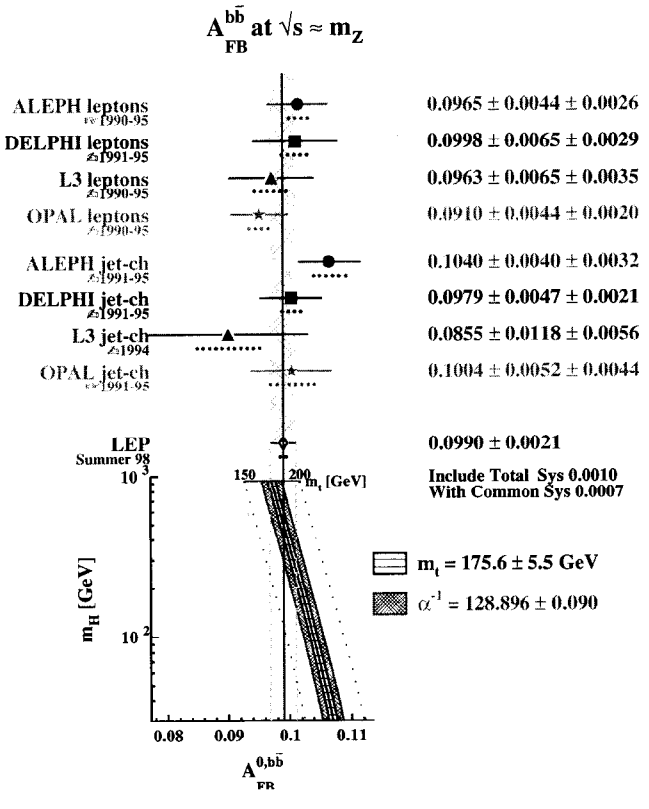

Fig. 4. The b-quark forward-backward charge asymmetry measured by the four experiments, together with the mean and the MSM prediction as a function of the top quark mass. The error bars reflect the full uncertainty.

the $D^{*\pm}$ meson. The results obtained by the four LEP collaborations with the different methods explained can be seen in Fig. 5.

The LEP results are combined at the "raw" asymmetry level, as measured at the average LEP energy and therefore, they have to be corrected for QED, QCD, and energy effects to obtain $A_{FB}^{0,q}$ as appearing in Eq. (15). After the corrections, and including the

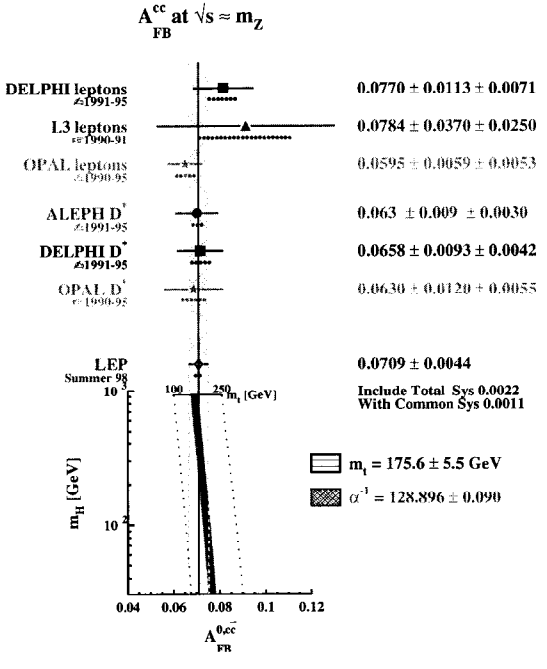

Fig. 5. The c-quark forward-backward charge asymmetry measured by the four experiments, together with the mean and the MSM prediction as a function of the top quark mass. The error bars reflect the full uncertainty.

relevant data from SLD as well, the results are

$$\begin{aligned} A_{FB}^{0,b} &= 0.0990 \pm 0.0021 \\ A_{FB}^{0,c} &= 0.0709 \pm 0.0044 \,. \end{aligned} \tag{16}$$

3 Interpretation of the Z Measurements

3.1 Direct Results

3.1.1 Tests of Lepton Universality

Lepton universality in the Z couplings can be tested by analyzing simultaneously the information coming from the lepton partial widths and the leptonic forward-backward and tau polarization asymmetries. Then, following Eqs. (4) and (7), the vector and axial couplings of the Z to each lepton species can be disentangled. The results (see Fig. 6) show perfect agreement with the hypothesis of lepton universality for both, the vector and axial couplings:

$$\begin{aligned} g_{A_\mu}/g_{A_e} &= 0.9996 \pm 0.0014 \\ g_{A_\tau}/g_{A_e} &= 1.0015 \pm 0.0015 \end{aligned}$$

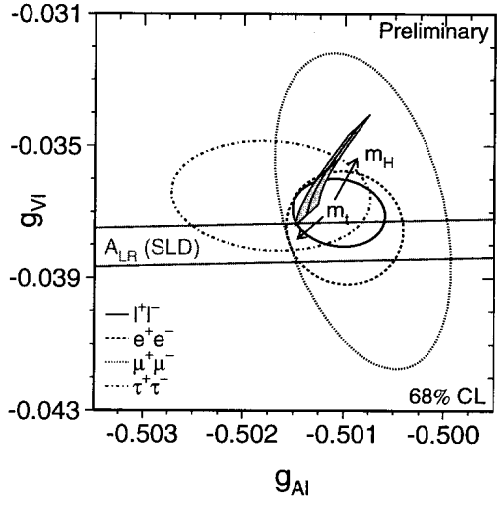

Fig. 6. The 68% probability contours in the g_{V_l}-g_{A_l} plane compared to the MSM predictions.

$$\begin{aligned} g_{V_\mu}/g_{V_e} &= 0.984 \pm 0.098 \\ g_{V_\tau}/g_{V_e} &= 0.974 \pm 0.043 \,. \end{aligned} \quad (17)$$

3.1.2 Tests of Z Couplings to Leptons and Quarks

Assuming lepton universality and using all the above asymmetry measurements, leptonic and hadronic, one can test whether the measured Z couplings to leptons and quarks do agree with their SM expectations or not. The combination of all the LEP leptonic asymmetries leads to a determination of the Z coupling to the leptons of

$$A_l = 0.1469 \pm 0.0027 \,.$$

As already explained, the quark asymmetries determined by LEP do not measure directly the quark couplings to the Z but instead their product with the leptonic ones. This is illustrated in Figs. 7 and 8 where the direct determination of A_b, A_c, and A_l performed at SLD by using initial state polarization is also shown. From these figures it is clear that no significant discrepancy with respect to the SM prediction can be claimed from the LEP measurements. Also, it is clear that the leptonic measurements lead to a value of A_l which in the SM requires a rather light Higgs, as we will see in more detail later.

3.1.3 The Effective Weak Mixing Angle

Figure 9 shows the compilation of all the values of $\sin^2\theta^{lept}_{eff}$ obtained from the asymmetry measurements at LEP presented in the previous sections. The SLD determination, coming from the measurement of the left-right polarization asymmetry,[6] is also shown. Its discrepancy with the average of the LEP measurements alone is about 2.1 σ. The overall agreement of all the measurements is reasonably good and the mean value provides a very precise determination of the effective weak mixing angle, which is very sensitive to the top quark and the Higgs masses.

Figure 10 summarizes the information coming from the measurement of the LEP asymmetries and the LEP lineshapes, and shows clearly the need for the existence of genuine electroweak radiative corrections beyond the running of the electromagnetic coupling constant to explain the measured values. It also shows that the uncertainty in $\Delta[1/\alpha(M_Z^2)] = 0.090$ that we'll assume throughout this note, has an impact in the interpretation of $\sin^2\theta^{lept}_{eff}$ comparable to the experimental error.

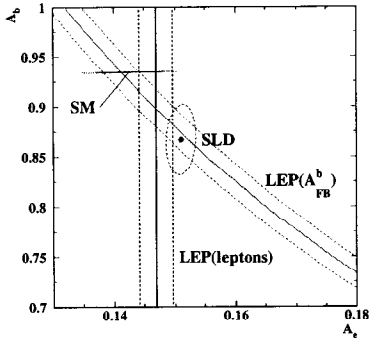

Fig. 7. One-sigma constraints in the A_b versus A_l plane coming from the leptonic and hadronic asymmetry measurements.

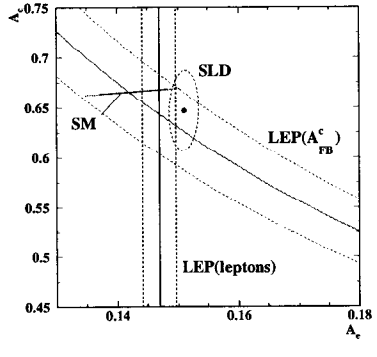

Fig. 8. One-sigma constraints in the A_c versus A_l plane coming from the leptonic and hadronic asymmetry measurements.

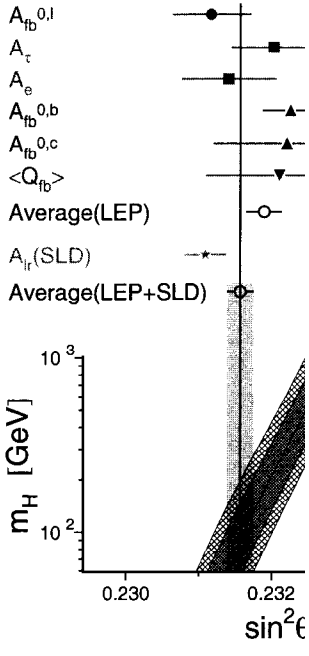

Fig. 9. The LEP averages for $\sin^2\theta^{lept}_{eff}$ obtain
ables discussed in the text, together with the S

3.1.4 Quantities Derived from Ratios

The ratios of partial widths, due to the cancela
numerator and denominator, allow the direct
the theory without relying, in principle, too
tensions of the MSM which would manifest
polarization would produce very similar predi

R_l depends little on m_t and M_H whereas
coupling constant, $R_l \sim R^0_l(1+\alpha_s(M_Z)/\pi)$. T
of $\alpha_s(M_Z)$ with minimum theoretical uncerta

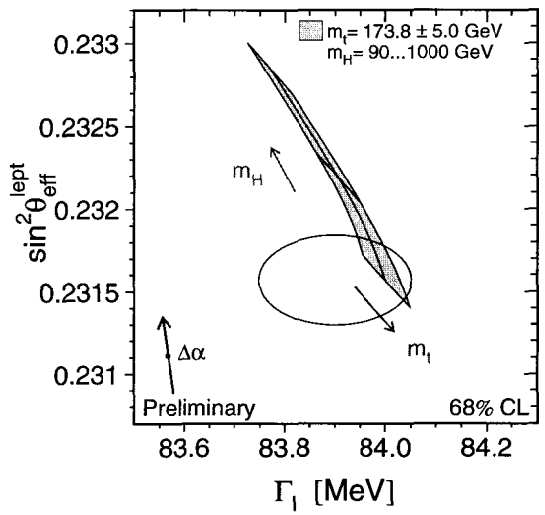

Fig. 10. The average for $\sin^2\theta^{lept}_{eff}$ and for Γ_l compared with the SM predictions. The arrow shows these predictions when the only electroweak radiative correction included is the running of the electromagnetic coupling constant.

using the formulae suggested in Ref. 8, which relate R_l to the QCD prediction, known to $\mathcal{O}(\alpha_s^3)$, one gets

$$\alpha_s(M_Z^2) = 0.122 \pm 0.004 \pm 0.001\ ,$$

where the second error accounts for varying M_H in the range, $M_H = 76^{+85}_{-47}$ GeV. This result is in good agreement with the world average, $\alpha_s(M_Z^2) = 0.119 \pm 0.002$.

The invisible width, Γ_{inv}, can be derived from the direct lineshape measurements by subtracting from the total width the one due to visible channels. If one assumes that all the invisible width is due to neutrino final states, then one can derive the number of light neutrino species N_ν by writing

$$\frac{\Gamma_{inv}}{\Gamma_l} = N_\nu \cdot \frac{\Gamma_\nu}{\Gamma_l} \qquad (18)$$

and taking the ratio Γ_ν over Γ_l from the MSM: $\Gamma_\nu/\Gamma_l = 1.991 \pm 0.001$. A small error should be noted in the MSM prediction for this ratio, which does not depend on α_s and in which the top and Higgs mass dependences largely cancel. Using the LEP average for $\Gamma_{inv}/\Gamma_l = 5.961 \pm 0.023$ one obtains

$$N_\nu = 2.994 \pm 0.011\ .$$

Since the result favors three species without any doubt, this measurement can then be interpreted as the determination of the width for additional invisible decays of the Z, which yields:

$$\Delta\Gamma_{inv} = -1.6 \pm 1.9\ \text{MeV}$$

or, equivalently

$$\Delta\Gamma_{inv} < 2.8\ \text{MeV}$$

at the 95 % confidence level.

4 The LEP-II Measurements

The LEP-I phase finished in 1995 and Table 1 shows the evolution of the center-of-mass energy in LEP after the LEP-II phase started, and the accumulated luminosity in each energy regime. Altogether, the data already analyzed amounts to less than 4000 W pairs. The data taken in 1998 is still being analyzed and therefore will not be covered in this note. The plans for the two forthcoming years are increasing the LEP energy as much as possible (up to 200 GeV) and taking as much luminosity as possible (about 100 pb^{-1}/exp./year).

Basically three different regimes can be distinguished in what concerns the LEP operation after the LEP-I phase:

- The so-called LEP 1.5 phase in which the energy was not sufficient for the production of W pairs and, hence the only relevant electroweak studies were those of the measurement of the γZ interference terms in the S-matrix language.
- In 1996 LEP raised the center-of-mass energy up to 161 GeV, reaching the threshold for the W-pair production and delivering about 40 pb^{-1} in total, which meant about 120 WW events. That "threshold regime" allowed, as we shall see, the indirect determination of the W mass through its effect on the observable cross section.

Table 1. The LEP center-of-mass energy and luminosity after the LEP-I phase.

Year	$\sqrt{s}$ (GeV)	$L(pb^{-1})$/exp.	W pairs
Nov. 1995	130/136 (LEP 1.5)	6	-
June-Aug. 1996	161 (WW threshold)	10	~ 30
Oct.-Nov. 1996	172	10	~ 100
July-Nov. 1997	183	55	~ 850
Nov. 1997	130/136	7	-
1998	189	~ 200	?

- After that, the increase in the LEP energy allowed the study of the WW cross section and asymmetries, independent of the direct measurement of their mass, by fitting the invariant mass distribution of their decay products.

These last two regimes are the relevant ones for the study of the W properties, which is the main electroweak subject of the LEP-II run. The other electroweak analyses with that data (mainly related to the Z events) are not going to be covered in this note.

The Ws are pair produced at LEP and, given the large W width, only their decay products can be detected. Ws are expected to decay into a lepton and a neutrino 33% of the time, and hadronically into jets 67% of the time. Therefore, the events observed at LEP can be classified into three categories:

- Fully Leptonic: ($BR = 11\%$), in which both Ws decay leptonically, leaving just two visible leptons. The events are characterized by a low multiplicity, high missing p_T, and large acoplanarity. Selection efficiencies are typically of about 70% for purities of about 90%. For this channel the backgrounds are not a big issue and come mainly from two-photon events and from radiative return Z leptonic decays (especially into taus) and at energies above the ZZ threshold from $ZZ \to l^+l^-\nu\bar{\nu}$ events.
- Semileptonic: ($BR = 44\%$), in which one W decays leptonically and the other decays hadronically. These events have large multiplicity, large missing p_T, and an isolated energetic lepton which should be rather antiparallel to the missing momentum direction. The selection efficiency is typically of the order of 85% for the lepton being an electron, 90% if it is a muon, and about 60% when it is a tau lepton, for purities well above 90%. The backgrounds for this channel are very low and come mainly from $q\bar{q}$ events, from Zee, and from other four-fermion processes.
- Fully hadronic: ($BR = 45\%$), in which both Ws decay hadronically, leading basically to four-jet events. The signature in this case is the high multiplicity and the nonexistence of missing mass. The background for this channel is rather severe, especially the one due to the process $q\bar{q} \to 4jets$ and therefore, the selection requires the use of the most sophisticated multivariable techniques (linear discriminant analyses, neural networks, etc.). The use of all sorts of kinematical variables, together with the use of variables related to lifetime tagging within these techniques (unlike the Zs, the Ws do not decay into b quarks), allow efficiencies above 80% for purities above 80%.

In the following sections we are going to describe how these different samples are used to determine the W boson parameters.

4.1 WW Cross Section and Branching Ratios

As already said, due to the extremely short W lifetime, only the four fermions coming from the W pair decay are observed in our detector. Therefore, in practice, all the possible ways in which these identified four fermions could come from the e^+e^- interaction should be considered as interfering channels to produce our detected final state. This interference which in principle could be large, can be drastically reduced by requiring the four fermions to be well inside the detector and well separated. Nevertheless, one needs a precise prescription to define what the WW cross section is and how can it be obtained from the measured four fermion cross section. The definition agreed among the four LEP collaborations corresponds to the diagrams depicted in Fig. 11 with the subsequent decay of the produced Ws:

$$\sigma_{WW} \equiv \sigma(e^+e^- \to W^+W^- \to 4f) \ ,$$

that is, the cross section through only the double W resonating diagrams (technically called CC03 diagram subset after the LEP-II workshop).[9]

The actual cross section measured by the LEP collaborations is corrected to this definition either by applying a correction factor or just by subtracting the remaining contributions estimated with a Monte Carlo simulation.

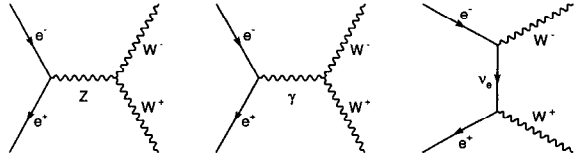

Fig. 11. The Feynman diagrams for the process, $e^+e^- \rightarrow W^+W^-$.

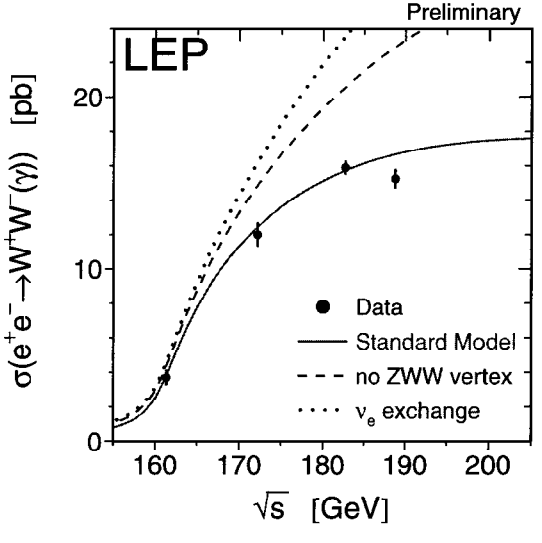

Fig. 12. The LEP average of the W pair cross section as a function of the center-of-mass energy compared with the SM prediction. The (very preliminary) measurement at 189 GeV is also shown. For illustration purposes the predictions neglecting the triple gauge coupling contributions are also given.

Figure 12 shows the LEP averaged total CC03 cross section as a function of the center-of-mass energy. The agreement with the SM expectation is excellent and excludes clearly a description in which the triple gauge coupling is neglected.

The analysis of the above cross sections for each individual channel allows the precise determination of the W branching ratios as can be seen from Figs. 13 and 14. In this second case, within the Standard Model, the branching ratio of the W bosons depends on the six elements of the Cabibbo-Kobayashi-Maskawa quark-mixing matrix (V_{CKM}) not involving the top quark and on α_s. Using the current world-averages and errors of other matrix elements, not assuming the unitarity of V_{CKM}, and from the world average of $\alpha_s(M_Z^2) = 0.119 \pm 0.002$ evolved to M_W^2, a constraint on the least well measured CKM matrix element is obtained:

$$|V_{cs}| = 1.04 \pm 0.04 \, .$$

4.2 W Mass

The W mass has been measured so far at LEP with the following two rather different techniques.

4.2.1 The Threshold Measurement

At threshold energies, the influence of the mass in the cross section is fundamentally a kinematic effect in the measured cross section which gives the highest sensitivity at about 161 GeV. The procedure to extract the W mass consists of the measurement of the cross section and its subsequent analysis in terms of the W mass using the most accurate theoretical predictions.[10] Although at these energies, no observable effects can be expected from the eventual existence of anomalous W couplings, it is true that one has to implicitly rely on the validity of the SM prediction of the cross section to extract the W mass. In this sense it is not a "model independent" measurement of M_W although it is free from some of the problems that affect other techniques.

4.2.2 The Direct Mass Reconstruction

Above threshold, the W mass is mainly obtained by the analysis of the invariant-mass distribution of the W decay products. This technique is only possible for semileptonic

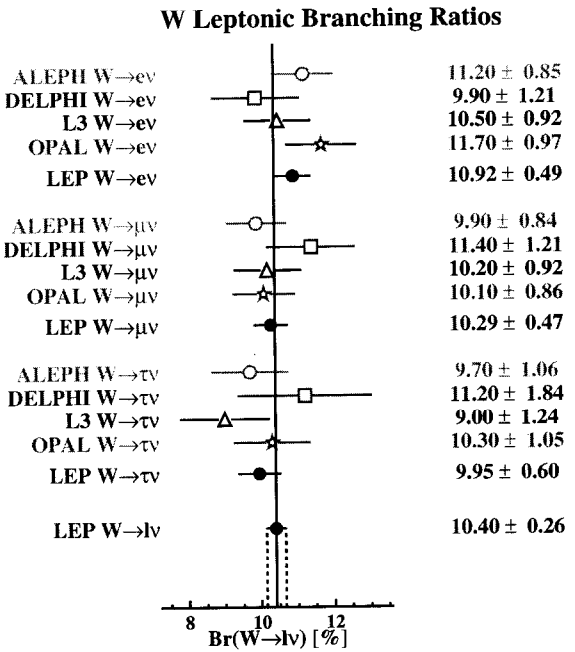

Fig. 13. The LEP measurements of the W leptonic branching ratios.

and fully hadronic events. In the first case, the events are forced to a two-jet configuration after excluding the lepton candidate. In the second case they are forced to a four (or more)-jet configuration using the jet algorithm giving the best invariant mass resolution.

In both cases, the invariant mass resolution is improved by applying a kinematical fit to reconstruct four objects using the energy and momentum constraints. The invariant mass resolution is further improved by constraining the two masses of the event to be (exactly or approximately) equal. This is called two-C fit in the semileptonic channel and five-C fit in the fully hadronic one.

In the fully hadronic case, the impossibility of unequivocally identifying the quark generating each jet introduces additional complications. Apart from the non-negligible

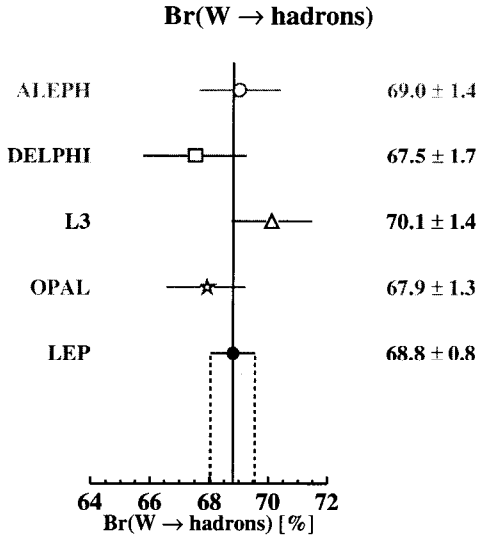

Fig. 14. The LEP measurements of the W hadronic branching ratios.

physics background already mentioned, the need for pairing the jets to determine the two W invariant masses introduces a non negligible combinatorial background which is reduced by the use of dedicated pairing algorithms.

After these steps, the invariant mass distributions have a Breit-Wigner like shape as can be seen in Figs. 15 and 16, but which is sizably distorted by several effects such as initial state radiation, phase space boundary, detector resolution, misassignment of particles to Ws, backgrounds, event selection, etc. Therefore, to get a precise determination of the W mass, elaborate fitting techniques should be applied to the reconstructed events. Out of the different techniques tried by the LEP experiments, one of the most popular is the use of Monte Carlo reconstructed mass distributions to compare directly with the data mass distributions. The idea is to have many large Monte Carlo template distributions generated with different W parameters to see which one fits the data best. Technically, instead of generating large MC samples at different W parameters, only a large sample is generated at a reasonable value of the W parameters (M_W^{MC}, Γ_W^{MC}) and

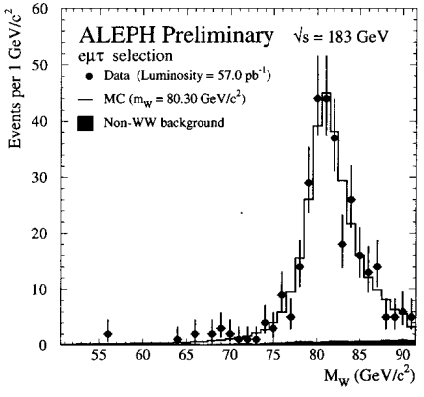

Fig. 15. The W reconstructed invariant mass distribution in semileptonic events.

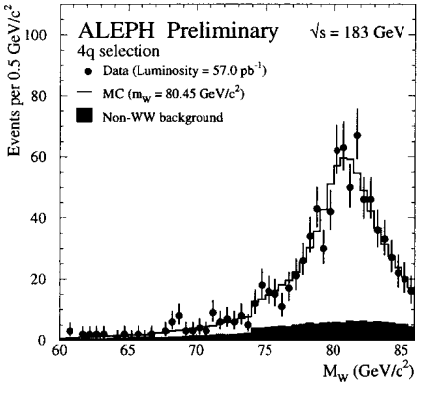

Fig. 16. The W reconstructed invariant mass distribution in fully hadronic events.

then the events are reweighted using the ratio of the matrix elements squared,

$$\omega_i(M_W, \Gamma_W) = \frac{|M(M_W, \Gamma_W; p_i^1, p_i^2, p_i^3, p_i^4)|}{|M(M_W^{MC}, \Gamma_W^{MC}; p_i^1, p_i^2, p_i^3, p_i^4)|}$$

to reproduce in a continuous manner the predictions for any other value of the W parameters with the same MC events.

In practice, from the fit to the invariant mass distributions, all the experiments extract M_W and some of them also Γ_W, though for this last parameter the present accuracy is still very poor.

4.2.3 Final State Interactions

An additional complication in the case of the fully hadronic channel is the fact that the expected separation of the W decay vertices ($1/\Gamma_W \sim 0.1$ fm) is smaller than the decay product hadronization scale [$\mathcal{O}(1\text{fm})$] so that the final state particle production cannot be expected to be dictated by the separate decays of the W bosons and therefore one may expect the identities of the individual W decay products not to be well defined any more. Two different kind of effects have been suggested as possible sources of W "crosstalking":

- The "color reconnection" between the quarks from different Ws. Since the Ws are color singlets, this effect is expected to be very small (a factor $\sim 1/N_c^2$ suppression) in the perturbative regime. Nevertheless it could, in principle, be sizable in the non-perturbative regime although, since in that regime there are no precise predictions, all we have are just phenomenological models which has just now started to be contrasted with the data. The models considered so far can be grouped into two families:
  - Color Singlet Models,[11] which predict mass shift effects ranging from zero to 50 MeV depending on the model parameters and the experimental procedure used.
  - Non-singlet Models,[12] which predict larger shifts but are already disfavored by the Z data and by the multiplicity distributions.
- The Bose-Einstein correlations between identical bosons (pions) from different Ws. As before, the expected mass shift depends on the model parameters[13] and on the experimental procedure used, and ranges from zero to about 50 MeV.

The detailed analysis of all the event properties should allow to discriminate between these models and to adjust their parameters independently from the W mass determination. Unfortunately, so far the statistical power of the data has been too limited to make any conclusive statement, although the preliminary results are encouraging and show the potential of the methods with the forthcoming statistics.

4.2.4 Results

The LEP results for the W mass determination, using the techniques explained above, are shown in Fig. 17. As can be seen, the most precise determination comes from the direct reconstruction and is in perfect agreement with the cross-section determination. Figure 18 shows that the LEP measurement is in good agreement with all the direct and indirect determinations of the W mass performed so far and that its accuracy is already comparable to the one obtained in the proton colliders, which so far were giving the best direct measurement.

In the direct reconstruction result, the uncertainty can be split as follows:

$$M_W = 80.32 \pm 0.08 \pm 0.05\,(FSI) \pm 0.02\,(LEP)\ \text{GeV}\,,$$

where the first term is the experimental uncertainty, FSI stands for the theoretical uncertainty due to Final State Interactions, and LEP stands for the uncertainty in the LEP center-of-mass energy. The direct reconstruction results for semileptonic and fully hadronic channels separately are:

$$\begin{aligned} M_W^{semileptonic} &= 80.31 \pm 0.11 \pm 0.02\,(LEP)\ \text{GeV} \\ M_W^{hadronic} &= 80.39 \pm 0.10 \pm 0.09\,(FSI) \pm 0.02\,(LEP)\ \text{GeV} \end{aligned}$$

so that no discrepancy pointing to an eventually large FSI effect is observed.

4.3 Triple Gauge Couplings

Since the couplings ZW^+W^- and γW^+W^- do enter at tree level in the prediction of the $e^+e^- \to W^+W^-$ cross section (see Fig. 11), LEP-II allows for the first time the direct study of the non-abelian structure of the electroweak SM in e^+e^- collisions.

The most general structure of the Lagrangian describing each one of these triple gauge couplings (TGC) which would preserve Lorentz invariance would have seven different terms, while in the Standard Model at tree level, just two terms for each coupling are predicted. Nevertheless, out of these seven terms, just three conserve C and P,

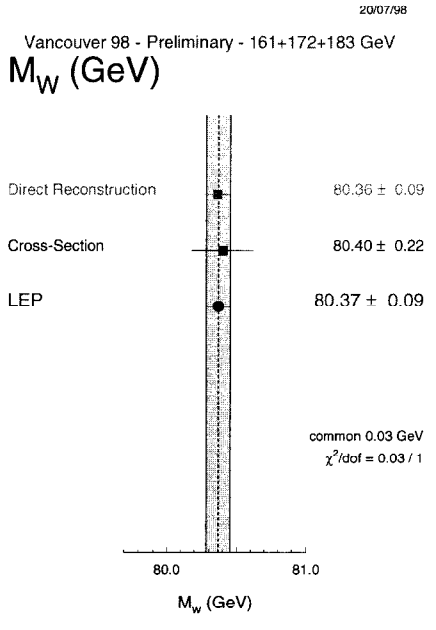

Fig. 17. The LEP determinations of the W mass.

while the other three violate CP and the last one just conserves CP. For several reasons to follow we will consider only those terms that conserve C and P, namely g_1, κ, and λ, which are related to the static electromagnetic moments for the W^+ in the following way:

$$\begin{aligned} Q_W &= eg_1^\gamma && \text{Electric charge} \\ \mu_W &= \tfrac{e}{2M_W}(g_1^\gamma + \kappa_\gamma + \lambda_\gamma) && \text{Magnetic dipole moment} \\ q_W &= -\tfrac{e}{M_W^2}(\kappa_\gamma - \lambda_\gamma) && \text{Electric quadrupole moment} \end{aligned}$$

and the same for the weak charge and moments by just substituting γ by Z. Any theory

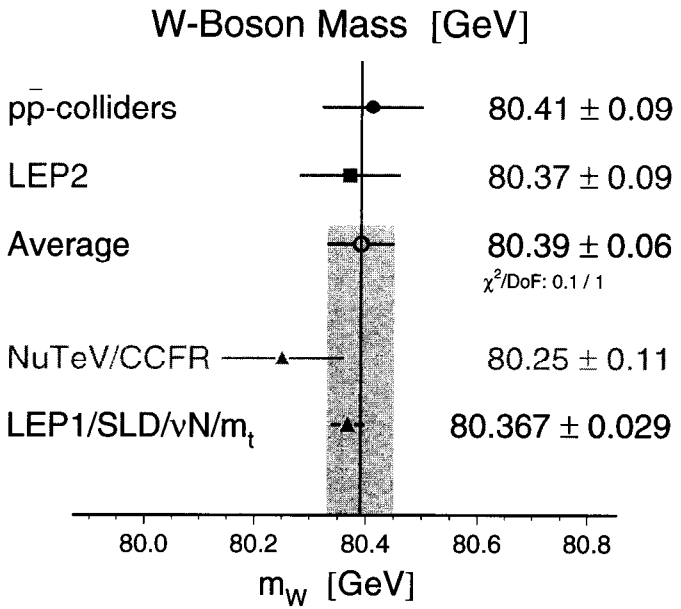

Fig. 18. Summary of all the determinations of the W mass.

incorporating new physics beyond the SM and including the electroweak theory as an effective low-energy limit may introduce deviations of these parameters from their SM values, which are:

$$\begin{aligned} g_1^\gamma &= g_1^Z = 1 \\ \kappa_\gamma &= \kappa_Z = 1 \\ \lambda_\gamma &= \lambda_Z = 0 \end{aligned}$$

so that the deviations can be quantified using $\Delta g_1 = g_1 - 1$, $\Delta\kappa = \kappa - 1$, and λ directly.

The assumption of electromagnetic gauge invariance reduces further the number of free parameters to five since it implies $g_1^\gamma = 1$ and, if in addition, global $SU(2)$ invariance is required, then the following relationship among these five parameters should hold:

$$\begin{aligned} \Delta\kappa_Z &= \Delta g_1^Z - \Delta\kappa_\gamma \tan^2\theta_W \\ \lambda_Z &= \lambda_\gamma \,. \end{aligned}$$

Therefore, we are left with just three free parameters which are Δg_1^Z, $\Delta\kappa_\gamma$, and λ_γ. Deviations of any of these three parameters from zero imply changes in the WW cross section, W production angles, W decay angles, and their correlations, which one can try to detect in the data.

For this purpose, so far only the semileptonic and fully hadronic channels are used. The selection and jet definition proceed typically in a similar way as for the mass determination. In the semileptonic events, the lepton charge is used to sign the W $\cos\theta$ direction and only a two-fold ambiguity remains to compute the decay angles in the hadronic W decay. In the fully hadronic case, the jet charge Q_{JET} is used to sign the W $\cos\theta$ direction and, on top of the combinatorial background already mentioned while discussing the mass determination, a four-fold ambiguity in the decay angles remains due to the two hadronic W decays. Due to these problems, the semileptonic channel is the most powerful one to study the triple gauge couplings.

A remaining problem is how to fit the mentioned three free parameters from the five-dimensional kinematical information, in addition to the total cross section. Several techniques have been developed in the different LEP collaborations which can be basically grouped as follows:

- Multidimensional Maximum Likelihood: It should allow to exploit the full angular information but in practice it is technically rather complex. Two approaches have been tried:
  - Unbinned using a semianalytical expression: It allows a relatively fast parameter fitting but requires afterwards, the application of rather involved multidimensional corrections in order to account for the biases and sensitivity losses introduced by backgrounds and experimental distortions.
  - Binned using Monte Carlo events: It incorporates properly all these corrections but requires a very large number of Monte Carlo events to be sure that all the bins in five-D do have significant population.
- Optimal Observables: The idea is to project the relevant kinematical information for a certain TGC observable onto a one-D distribution. Since triple gauge cou-

plings contribute at tree level only linearly to the process amplitude, they show up in the differential cross section as a quadratic effect:

$$\frac{d\sigma(\Omega,\bar{\alpha})}{d\Omega} = S_0(\Omega) + \sum_i S_{1;i}(\Omega)\,\alpha_i + \sum_{i,j} S_{2;i,j}(\Omega)\,\alpha_i\alpha_j\ ,$$

where α_i stands for the couplings and Ω stands for the observed kinematical variables. From this simple equation it can be shown that the optimal observable for coupling "i" can be defined as:

$$OO_i \equiv \frac{\frac{d}{d\alpha_i}\left(\frac{d\sigma(\Omega,\bar{\alpha})}{d\Omega}\right)|_{\alpha_i=0}}{\frac{d\sigma(\Omega,\bar{\alpha})}{d\Omega}|_{\alpha_i=0}} = \frac{S_{1;i}(\Omega)}{S_0(\Omega)}\ .$$

In practice, the Monte Carlo $d\sigma/d\Omega$ is used to account for the backgrounds and experimental effects, and the parameters are extracted by computing the value of the probability of the observed value of the OO_i for each event and then maximizing their combined likelihood function.

By now, given the limited statistical power of the measurements, the results from the different LEP experiments are provided as likelihood curves for a single parameter fit while the other parameters are zeroed. These likelihood curves are then combined, as can be seen in Fig. 19. From the results collected in that figure, no significant discrepancy with the SM is observed.

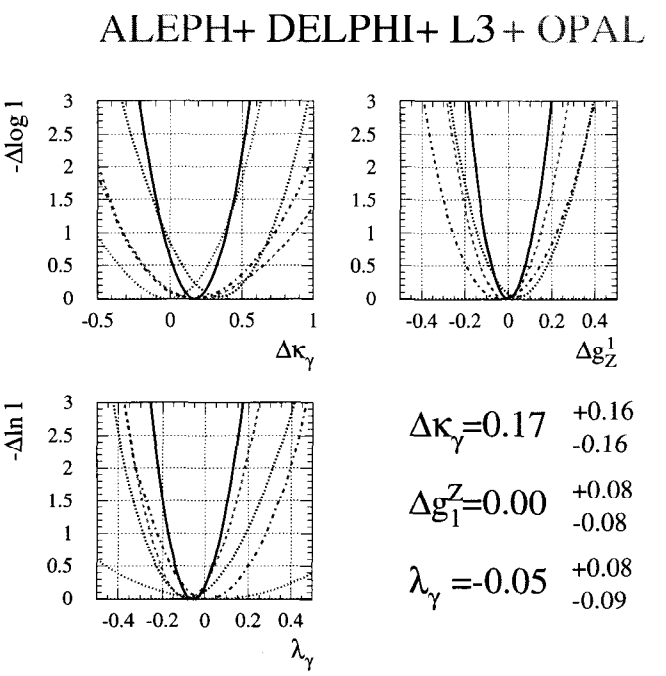

Fig. 19. Summary of the LEP constraints on the triple gauge couplings.

5 Standard Model Fits

The results presented in the previous sections can be interpreted in the context of the MSM, allowing a check of its validity in describing all the observations, and enabling the inference of some of the fundamental MSM parameters.

The comparison is made through a fit of the measurements shown in Table 2 to their MSM predictions in terms of the top quark mass m_t, the Higgs boson mass M_H, and the value of $\alpha_s(M_Z)$.

The most up-to-date MSM calculations have been used and their estimated theoretical uncertainties[14] have also been propagated in the fitting procedure. The uncertainty in $1/\alpha(M_Z^2) = 128.878 \pm 0.090$,[15] due to the contribution of light quarks in the photon vacuum-polarization, is the one that dominates by far.

The results of the fit with different data sets are presented in Table 3. It is clear from these results that the data prefers a rather light Higgs boson mass as can be seen also in Fig. 20. In that figure, the impact of taking $1/\alpha(M_Z^2) = 128.905 \pm 0.036$, as advocated in Ref. 16, is also shown.

In addition, from Table 3 one sees that there is a nice agreement between the direct measurement of m_t and M_W and their indirect determination through their effect in the precision electroweak measurements. This fact constitutes a successful deep test of the Standard Model predictions beyond the tree level structure. This agreement can also be seen in Fig. 21 which also illustrates the fact mentioned above: in a completely independent manner, the precision electroweak measurements and the direct determinations of m_t and M_W point to a rather light Higgs boson mass.

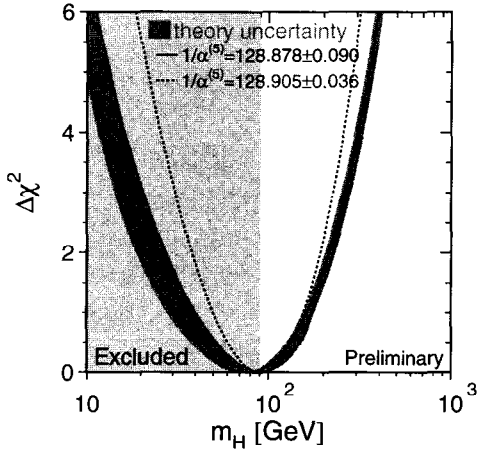

Fig. 20. $\Delta\chi^2$ vs $M_{\rm H}$ using all data.

	Measurement	Correlation Matrix	Standard Model Fit	Pull
$\alpha(M_Z^2)^{-1}$	$128.878 \pm 0.090(83)$		128.878	0.0
a) LEP				
line-shape and				
lepton asymm.:				
M_Z [GeV]	$91.1867 \pm 0.0021(17)$	1.00	91.1865	0.1
Γ_Z [GeV]	$2.4939 \pm 0.0024(13)$	0.00 1.00	2.4958	−0.8
σ_h^0 [nb]	$41.491 \pm 0.058(57)$	-0.04 -0.18 1.00	41.473	0.3
R_l	$20.765 \pm 0.026(20)$	-0.01 0.00 0.12 1.00	20.748	0.7
$A_{FB}^{0,l}$	$0.01683 \pm 0.00096(60)$	0.06 0.00 0.01 -0.07 1.00	0.01613	0.7
τ polarization:				
A_τ	$0.1431 \pm 0.0045(27)$		0.1467	−0.8
A_e	$0.1479 \pm 0.0051(10)$		0.1467	0.2
b and c quark:				
R_b^0	$0.21656 \pm 0.00074(57)$	1.00	0.21590	0.9
R_c^0	$0.1735 \pm 0.0044(34)$	-0.17 1.00	0.1722	0.3
$A_{FB}^{0,b}$	$0.0990 \pm 0.0021(10)$	-0.06 0.05 1.00	0.1028	−1.8
$A_{FB}^{0,c}$	$0.0709 \pm 0.0044(22)$	0.02 -0.04 0.13 1.00	0.0734	−0.6
$q\bar{q}$ charge asymm.:				
$\sin^2\theta_{eff}^{lept}(Q_{FB})$	$0.2321 \pm 0.0010(8)$		0.23157	0.5
M_W [GeV]	$80.37 \pm 0.09(6)$		80.37	0.0
b) SLD				
$\sin^2\theta_{eff}^{lept}(A_{LR})$	$0.23109 \pm 0.00029(18)$		0.23157	−1.7
A_b	$0.867 \pm 0.035(25)$		0.935	−1.9
A_c	$0.647 \pm 0.040(23)$		0.668	−0.5
c) $p\bar{p}$ and νN				
M_W [GeV] ($p\bar{p}$)	$80.41 \pm 0.09(07)$		80.37	0.4
$1 - M_W^2/M_Z^2(\nu N)$	$0.2254 \pm 0.0021(10)$		0.2232	1.1
m_t [GeV] ($p\bar{p}$)	$173.8 \pm 5.0(3.9)$		171.1	0.5

Table 2. Summary of measurements included in the combined analysis of SM parameters. Section a) summarizes LEP averages (which in the case of R_b and R_c, also include SLD); section b) summarizes the relevant additional SLD results; and section c) summarizes the electroweak results from hadron colliders and νN-scattering. The size of the estimated systematic component of the quoted uncertainty is indicated in parentheses. The MSM fit result in column three and the pulls in column four are derived from the fit including all data with the Higgs mass as a free parameter.

Table 3. Results of fits to LEP and other data for m_t, M_H, and $\alpha_s(M_Z^2)$. No external constraint on $\alpha_s(M_Z^2)$ has been imposed.

	LEP	No M_W,no m_t	No M_W	All data
m_t (GeV)	$160\ ^{+13}_{-9}$	$158\ ^{+9}_{-8}$	171.0 ± 4.9	151.1 ± 4.9
M_H (GeV)	$60\ ^{+127}_{-35}$	$32\ ^{+41}_{-15}$	$82\ ^{+95}_{-51}$	$76\ ^{+85}_{-47}$
$\alpha_s(M_Z^2)$	0.121 ± 0.003	0.120 ± 0.003	0.120 ± 0.003	0.119 ± 0.003
$\chi^2/(d.o.f.)$	4/9	13/12	15/13	15/15
$\sin^2\theta^{lept}_{eff}$	0.23182 ± 0.00023	0.23157 ± 0.00018	0.23159 ± 0.00020	0.23157 ± 0.00019
M_W (GeV)	80.314 ± 0.038	80.332 ± 0.037	80.367 ± 0.029	80.371 ± 0.026

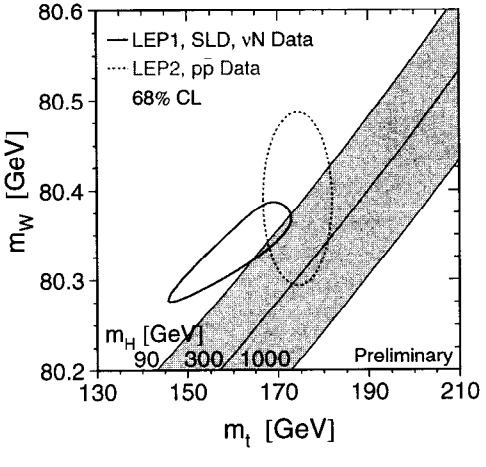

Fig. 21. The direct and indirect determinations of m_t and M_W compared with the SM predictions.

6 Summary

The precision electroweak measurements at LEP-I have been a big success, even beyond the most optimistic expectations. Thanks to these measurements, the Z boson properties are known today with very high precision.

The LEP-II electroweak precision program started just a few years ago and is now reaching maturity. The most precise measurement, M_W, has already reached the same precision as in collider experiments. The statistics accumulated during 1998 and the ones foreseen in the coming years should also allow precision measurements of the rest of the W boson properties.

Altogether, these measurements allow an unprecedented test of the good health of the MSM in describing the electroweak data and, together with the relevant electroweak measurements performed around the world, open a significant window for the inference of the last missing piece of the puzzle: M_H.

References

[1] M. Martinez *et al.*, "Precision Tests of the Electroweak Interaction and the Z Pole," Rev. Mod. Phys. **71**, 575 (1999).

[2] The LEP Electroweak Working Group, "A Combination of Preliminary Electroweak Measurements and Constraints on the Standard Model," CERN-EP/99-015, February 1999. Prepared from Contributions of the LEP and SLD Experiments to the 1998 summer conferences.

[3] The LEP Energy Working Group, "Calibration of the Center-of-Mass Energies at LEP1 for Precise Measurements of Z Properties," Eur. Phys. J. C **6**, 187 (1999).

[4] S. Jadach *et al.*, "New Results on the Theoretical Precision of the LEP/SLC Luminosity," Phys. Lett. B **450**, 262 (1999).

[5] A. Leike, T. Riemann, and J. Rose, Phys. Lett. B **273**, 513 (1991); T. Riemann, Phys. Lett. B **293**, 451 (1992); S. Kirsh and T. Riemann, Comput. Phys. Commun. **88**, 89 (1995).

[6] K. Baird for the SLD Collaboration, "Measurements of A_{LR} and A_l from SLD," talk presented at ICHEP 98, Vancouver, B.C., Canada, 23–29 July 1998.

[7] The LEP Heavy Flavor Group, "Input Parameters for the LEP/SLD Electroweak Heavy Flavor Results for Summer 1998 Conferences," Internal note LEPHF/98-01, "http://www.cern.ch/LEPEWWG/heavy/lephf9801.ps.gz."

[8] T. Hebbeker *et al.*, Phys. Lett. B **331**, 165 (1994); P. A. Raczka and A. Szymacha, Phys. Rev. D **54**, 3073 (1996); D. E. Soper and L. R. Surguladze, Phys. Rev. D **54**, 4566 (1996).

[9] "Physics at LEP2," edited by G. Altarelli, T. Sjöstrand, and F. Zwirner, CERN 96-01 Yellow Report, Vol. 1, February 1996.

[10] D. Bardin, *et al.*, Nucl. Phys. B (Proc. Suppl.) **37**, 148 (1994); S. Jadach *et al.*, Comput. Phys. Commun. **94**, 216 (1996).

[11] T. Sjöstrand and V. A. Khoze, Z. Phys. C **62**, 281 (1994); L. Lönnblad and T. Sjöstrand, Phys. Lett. B **351**, 293 (1995); V. A. Khoze and T. Sjöstrand, Eur. Phys. J. C **6**, 271 (1999) and references therein.

[12] J. Ellis and K. Geiger, Phys. Lett. B **504**, 230 (1997).

[13] S. Jadach and K. Zalewski, CERN-TH/97-29, Acta Phys. Polon. B **28**, 1363 (1997).

[14] D. Bardin *et al.*,"Precision Calculation Working Group" (PCWG), CERN 95-03 Yellow Report, 31 March 1995 and references therein; D. Bardin and G. Passarino, "Upgrading of Precision Calculations for Electroweak Observables," CERN-TH/98-92 [hep-ph/9803425].

[15] S. Eidelmann and F. Jegerlehner, Z. Phys. C **67**, 585 (1995); H. Burkhardt and B. Pietrzyk, Phys. Lett. B **356**, 398 (1995).

[16] M. Davier and A. Höcker, Phys. Lett. B **419**, 419 (1998).